Disponible en **www.hormigonyacero.com**
Hormigón y Acero 2024
https://doi.org/10.33586/hya.2023.3122

A Study on the Distribution of Shear Forces Between Resisting Mechanisms in a RC Element Without Stirrups

Estudio de la distribución del esfuerzo cortante entre distintos mecanismos resistentes en un elemento de hormigón armado sin armadura transversal

Alejandro Pérez Caldentey[a,*]

[a] *Universidad Politécnica de Madrid. Prof. Aranguren S/N. 28040 Madrid, SPAIN*
FHECOR Consulting Engineers. Barquillo, 23, 2º. 28004 Madrid, SPAIN..

Recibido el 28 de diciembre de 2022; revisado el 7 de julio de 2023, aceptado el 11 de julio de 2023

ABSTRACT

This paper explores how the shear force distributes itself among the three main shear resistance mechanisms: shear resistance of the uncracked compressed chord, aggregate interlock, and dowel effect. Today's dominating shear models, the critical crack theory (Muttoni *et al.* [1]) and the compression field theory (Collins *et al.* [2]) maintain that the main shear-resisting mechanism is aggregate interlock, while more recent studies (Marí *et al.* [3]), maintain that the main resistance mechanism is the shear resistance on the uncracked compression chord.

In this paper FEM modelling is used to study a test carried out at the Universidad Politécnica de Madrid (UPM) to try to assign the shear force to the different shear mechanisms for different loading steps and elucidate what finally causes the failure of the structure. The results show that as load is increased the relative part of the shear force taken by the uncracked compressed chord increases until, finally, shear failure is reached when the principal tensile stress in the area located close to the load but towards the support reaches the tensile resistance of concrete, generating a crack that precipitates the failure of the beam.

It should be pointed out that the study included in this paper is only preliminary and should be extended to other cases exploring different sizes, reinforcement ratios, etc.

KEYWORDS: physical model, shear resistance mechanisms, elements without shear reinforcement.

RESUMEN

Este artículo explora cómo se distribuye el esfuerzo cortante entre los tres mecanismos principales de resistencia a cortante: resistencia del cordón comprimido, engranamiento de los áridos y efecto pasador. Los modelos de resistencia a cortante dominantes en la actualidad, la teoría de la fisura crítica (Muttoni *et al.* [1]) y la teoría del campo de compresiones (Collins *et al.* [2]), sostienen que el principal mecanismo de resistencia a cortante es el engranamiento de los áridos, mientras que estudios más recientes (Marí *et al.* [3]), sostienen que el principal mecanismo de resistencia es la capacidad a cortante de la cabeza comprimida.

En este trabajo se utiliza un modelo de elementos finitos para estudiar un ensayo realizado en la Universidad Politécnica de Madrid (UPM) para tratar de asignar la fuerza cortante a los diferentes mecanismos de cortante para diferentes escalones de carga y dilucidar qué es lo que finalmente provoca el fallo de la estructura. Los resultados muestran que a medida que se incrementa la carga aumenta la parte relativa del esfuerzo cortante que toma el cordón comprimido no fisurado hasta que finalmente se alcanza el fallo por cortante cuando el esfuerzo principal de tracción en la zona situada cerca de la carga, pero hacia el apoyo alcanza la resistencia a tracción del hormigón, generando una fisura que precipita el fallo de la viga.

Hay que señalar que el estudio incluido en este trabajo es sólo preliminar y debería ampliarse a otros casos explorando diferentes tamaños, cuantías de armadura, etc.

PALABRAS CLAVE: modelo físico, mecanismos de resistencia a cortante, elementos sin armadura de cortante.

* Persona de contacto / *Corresponding author*:
Correo-e / *e-mail*: apc@fhecor.es (Alejandro Pérez Caldentey)

How to cite this article: Pérez, A. (2024) A Study on the Distribution of Shear Forces Between Resisting Mechanisms in a RC Element without Stirrups, *Hormigón y Acero* 75(302-303): 109-118. https://doi.org/10.33586/hya.2023.3122

1. INTRODUCTION

The distribution of shear among the several identified mechanisms which explain the shear resistance of reinforced concrete elements in shear has been studied by many researchers. The main mechanisms identified are:

- The shear resisted by the uncracked compression chord
- The shear resistance taken by aggregate interlock and resi-

dual tensile strength
- The shear resisted by dowel effect
- The shear resisted by direct transmission of forces (arch effect)

Researchers have tried to separate these mechanisms by ingenious testing to quantify the effect of each mechanism separately. While the consideration of shear resisted by the uncracked compression chord has been treated mostly on a theoretical level (mainly by computing the tensile principal stress), a considerable number of tests have been carried out to evaluate aggregate interlock. Among these are the tests carried out by Fenwick and Paulay [4], Taylor [5] [6], and Walraven [7] [8]. Walraven's formulation was later simplified to allow for a closed form expression by Cavagnis *et al.* [9].
While work by Vecchio and Collins is also predominant in this area ([2], [10]), it is based on the tests of reinforced concrete panels [10] and in the author's opinion they do not properly model what goes on inside a slab where there is no distributed longitudinal reinforcement spaced along the vertical direction to control crack width. For this reason, the expressions derived from these tests would tend to overestimate the shear resistance of slabs without shear reinforcement.

The dowel effect has been the object of experimental studies by Krefeld and Thurston [11], Fenwick and Paulay [4], Baumann [12] and Taylor [5]. From the analysis of these tests it is fairly clear that the dowel effect can absorb significant shear forces, when considered as an isolated mechanism. For instance, the shear force resisted by the dowel effect in the beams tested by Krefeld and Thurston having 30 cm of height (d=25 cm) and 15 cm of width, with a fairly low concrete strength (18 MPa) was around 16 kN, which would amount to a shear stress of 0.4 MPa. However, it will be shown that the small stiffness of the mechanism leads to the absorption of a very small part of the shear force during the loading process and the brittle behaviour of the compressed chord does not allow for redistribution of forces towards this mechanism that would allow a significant contribution from it.

The arch effect, which is significant in practical cases but mostly neglected in code models was of course first studied in-depth by Kani [13]. This effect will not be analysed in this paper and therefore no further discussion on it will be made.

While the study of the independent resisting mechanisms is interesting and worthwhile, it does not answer the question of what the shear resistance of a beam would be since the different mechanisms take a part of the load depending on stiffness considerations and the brittleness of the mechanisms leads to failure of the specimen before the maximum capacity of all mechanisms is achieved. Analyses studying the interaction of the different mechanisms have been carried out by different researchers. For instance, Reineck [14] uses constitutive laws for the different resistance mechanisms. However, the kinematic assumption made by Reineck and related to the shape of the crack is questionable. Instead of following a realistic shape of the actual critical shear crack that forms in tests, Reineck assumes that the crack does not propagate backwards, and that the displacement of the crack lips can be modelled by rotation from the end of the crack at the compression chord (see Figure 1). This is not what is observed in actual tests and a different kinematic assumption will be made in this paper.

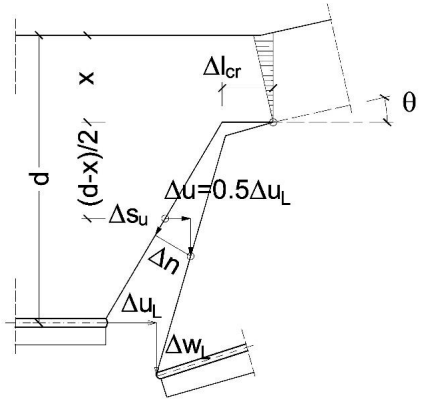

Figure 1. Kinematic assumption made by Reineck, redrawn and adapted from [14].

Monserrat [15], also includes a sophisticated model for the different mechanisms and obtains values for the contribution of the different mechanisms for the tests carried out for her PhD thesis. In this document she included not only the mechanisms mentioned above but also the dowel effect of compression reinforcement, which is significant when this reinforcement is below the neutral axis (in fact this is related to the effect of longitudinal skin reinforcement as assumed by Vecchio and Collins), residual tensile stress, and the contribution of the stirrups. Her approach is different, and results in a significant contribution of the dowel effect of both the top and bottom reinforcements. It will be shown below that the dowel effect in the case studied in this paper is very small.

More recent work includes other variables such as the influence of time-dependent effects [16], the influence of time dependent effects plus corrosion [17], the influence of the slenderness of the cross section [18], the effect of axial forces [19], while others are trying to apply artificial intelligence to predict shear resistance [20], [21].

2. DESCRIPTION OF HOW THE CRACK FORMS AND PROGRESSES AND HOW FAILURE OCCURS

There are two classical types of shear failure in elements without stirrups:
- The flexural-shear failure, in which the shear crack originates from a pre-existing flexural crack. The flexural crack progresses vertically up to the uncracked centroid of the section where it becomes inclined (first at 45º) with decreasing slope until it becomes fairly horizontal as it reaches the cracked neutral axis. Simultaneously the crack propagates towards the support in a similar manner, eventually becoming parallel to the tension reinforcement.
  This type of failure originates when the shear load is sufficiently far away from the support so that bending forces are significant. This type of crack can be approximately described by using a geometry consisting in two parabolas which are tangent at the centroid of the section (provided there are no axial forces).
- The direct tension shear failure, which originates at the fibre with the highest shear stress (i.e., at the centroid of the uncracked section if there are no axial forces). In this case,

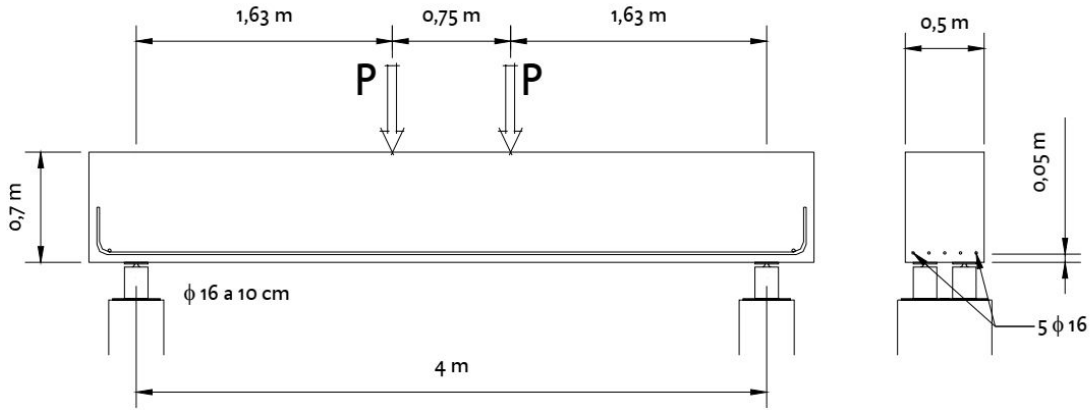

Figure 2. Tests setup and cross section dimensions.

Figure 3. View of specimen after failure.

the shear crack is fairly straight and connects the shear load to the support. This type of shear crack can also be typical of prestressed members.

In this paper a detailed analysis of the first type of failure will be presented, using a test carried out at the Universidad Politécnica de Madrid and documented in [22]: test 70-3.1-I-2P.

3. TEST DESCRIPTION

Test 70-3.1-I-2P, is a shear test of a simply supported beam with a span of 4.00 meters subjected to 2-point loads spaced 0.75 m apart. The cross section is rectangular with a 50 cm width and a 70 cm height and is reinforced with 5ϕ16 mm bars. The concrete was tested at 28 days and had a mean compressive strength of 43.5 MPa, a mean tensile strength of 3.8 MPa and an elastic modulus of 28950 MPa. The dimensions of the cross section and the test set-up is shown in Figure 2. Failure occurred for a value of the load P equal to 230 kN. Figure 3 shows a view of the specimen after failure. The shape of the crack is typical of a flexural-shear failure. Note the cracking that occurs at the top of the of the section to the left of the point of application of the load.

4. FEM MODELLING

For the simulation of tests 70-3.1-I-2P, a 2-D finite element model has been developed using the software SOFISTIK, using 4-node QUAD elements. The model has been generated using a python code for ease of generation and to enable the study of sensitivity to discretization and the future extension of the study to other specific cases. The model assumes the shape of the crack as two tangent parabolas with a length equal to two times its height and with the point of tangency located at the centroid of the uncracked cross section (see point C in Figure 4). The definition of the shape of the crack is given in Eq. (1) .

$$y = r + \frac{1}{4(d-y_g)}\left(x-a-2(d-y)\right)^2 \qquad a-2(d-y)\le x\le a-2(d-y_g)$$
$$y = d-y\,\frac{1}{4(y_g-y)}(x-a)^2 \qquad a-2(d-y_g)\le x\le a \tag{1}$$

where:

- y,x are the cordinates of the parabola with respect to the origin taken as the point located at the bottom of the section at its intersection with the left support
- d is the effective height
- y_g is distance from the top fibre to the centroid of the uncracked section
- a is the distance of load P to the support
- r is the distance of the centroid of the tension reinforcement to the bottom fibre

The lips of the crack are bridged vertically and horizontally by nonlinear truss elements whose constitutive laws will be described further on. The constitutive law considered for concrete is a Sargin law in compression (with a mean compressive strength of 43.5 MPa) together with a linear branch in tension up to the sustained tensile strength ($k_{ct} f_{ctm}$=0.7f_{ctm}=2.66 MPa). As steel does not yield, a linear constitutive law has been assumed both in tension and compression with a modulus of elasticity of 200000 MPa.

The reinforcement is modelled using a thin layer of QUAD elements. The height of this layer is determined so that is has the same inertia of the actual bars to better model the dowel effect. This leads to an area which is not the actual area of the reinforcement. This however does not have a significant bea-

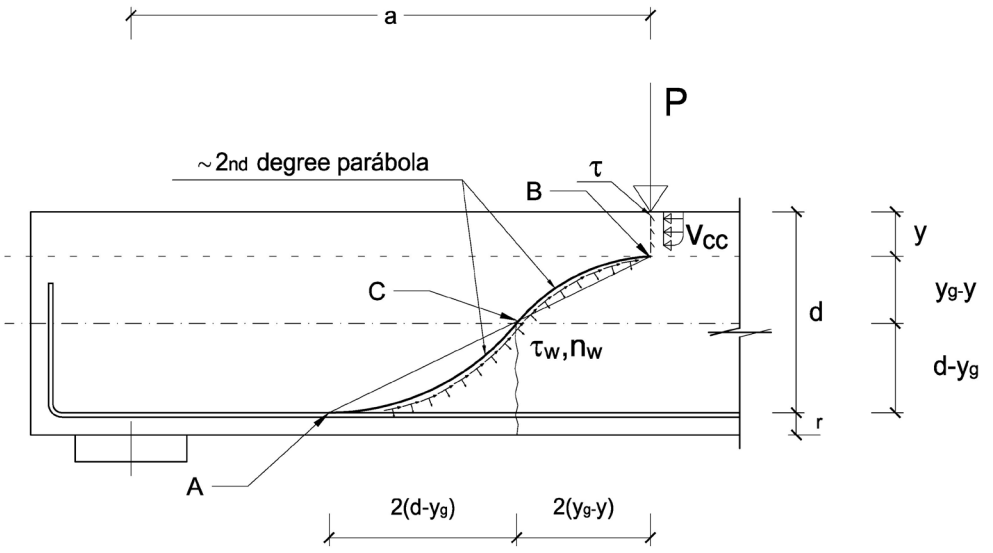

Figure 4. Crack location and symbol definition.

ring on the results because the behaviour of steel stays within the linear elastic range.

Figure 5 shows a view of the pre-cracked FEM model. Note that in this model the springs have a resistance that accounts for the tensile strength of concrete, so that the crack only opens as the tensile resistance is overcome. So the crack is not active from the beginning, but forms as the load is applied along the predefined path. Additionally, another model without the non-linear springs is also used to evaluate the behaviour of an element without aggregate interlock. While the first model fails for a load very close to the experimental value of 230 kN (+10% →253 kN), the model without the aggregate interlock effect fails for a load of about 80% of the measured value (184 kN). For loads larger than the ones mentioned, failure occurs due to tension stresses in concrete developing in the area to the left of the point of application of the load. In fact, a sort of cantilever develops to the left of the applied load which is subjected to the axial load from integral of stresses in the compressed chord and bending from both the eccentricity of the normal forces with respect to the centroid of the resisting section and from the eccentricity of the applied load, as shown in Figure 7. When the principal tensile stress reaches the assumed tensile strength of concrete for sustained loading ($k_{ct} f_{ctm}$=0.7f_{ctm}) at the critical section, failure occurs. Eq. (2) shows a simplified evaluation of this situation, which assumes that Navier's hypothesis is verified at the critical section, which is a simplification.

$$N = C$$
$$M = C\Delta y - P\Delta x$$
$$V = V_{cc}$$
$$\sigma_x(y) = \frac{N}{b h_{crit}} - \frac{M\left(\frac{h_{crit}}{2} - y\right)}{\frac{b h_{crit}^2}{12}} \qquad (2)$$
$$\tau(y) = \frac{V_{cc} b y \left(\frac{h_{crit}}{2} - \frac{y}{2}\right)}{\frac{1}{12} b h_{crit}^2 b}$$
$$\sigma_{II} = \min\left(\frac{\sigma_x(y)}{2} - \sqrt{\left(\frac{\sigma_x(y)}{2}\right) + \tau(y)^2}\right) = -k_{ct} f_{ctm} \rightarrow failure$$

where:

- N,M are the normal forces applied on the critical section
- V is the shear force applied on the critical section
- C is the integral of the compressive stresses in the compression chord at the section of the applied load P.
- Δ is the eccentricity of force C with respect to the centroid of the critical section
- Δx is the horizontal distance between the section at which force P is applied and the critical section
- V_{cc} is the shear force resisted by the compression chord
- $\sigma_x(y)$ is the normal stress at a distance y from the top fibre at the critical section
- $\tau\,(y)$ is the shear stress at a distance y from the top fibre at the critical section
- h_{crit} is height of the critical section
- $\sigma_{II}(y)$ is the principal tensile stress at a distance y from the top fibre at the critical section
- f_{ctm} is the mean tensile strength of concrete
- k_{ct} is the reduction factor for tensile strength due to sustained loading (taken as 0.7)

For the tangential and normal forces of the springs along the crack, the formulation of Cavagnis *et al.* [9], mentioned above, is used (see Eq. (3))

$$\tau_w = \sqrt{f_{cm}} \frac{35\left(\frac{\Delta}{d_{dg}}\right)^{\frac{4}{3}}}{\left(40\frac{w}{d_{dg}}\right)^{1.8+40\frac{\delta}{d_{dg}}}}$$
$$\sigma_w = \sqrt{f_{cm}} \frac{400\left(\frac{\Delta}{d_{dg}}\right)^{\frac{7}{3}}}{\left(40\frac{w}{d_{dg}}\right)^{3+40\frac{\delta}{d_{dg}}}} \qquad (3)$$

where:

- w is the crack width
- Δ is the relative slip between the two crack edges
- d_{dg} is a parameter accounting for the maximum aggregate size: d_{dg}=d_{max}+16
- f_{cm} is the mean compressive concrete strength

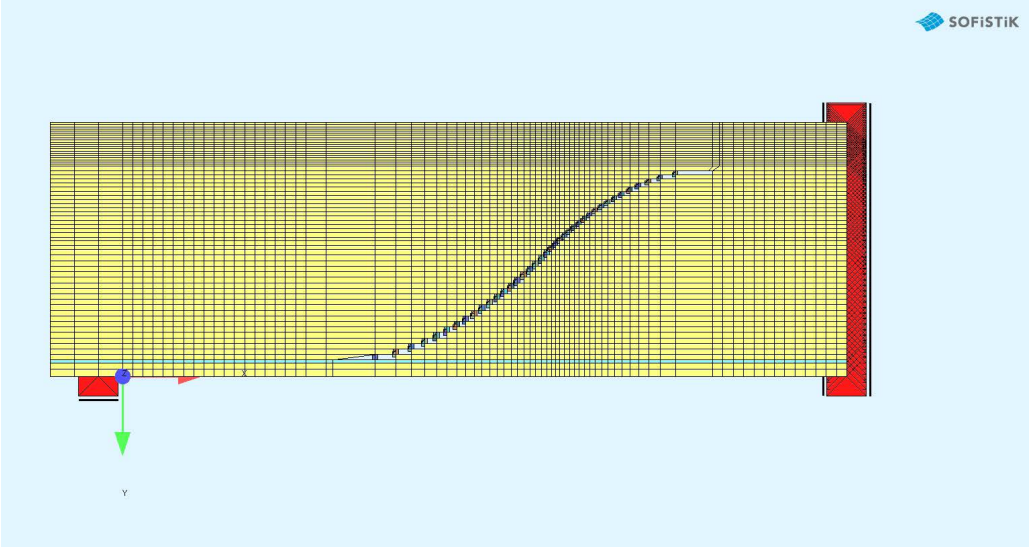

Figure 5. FEM Model with non-linear truss elements bridging the crack both vertically and horizontally.

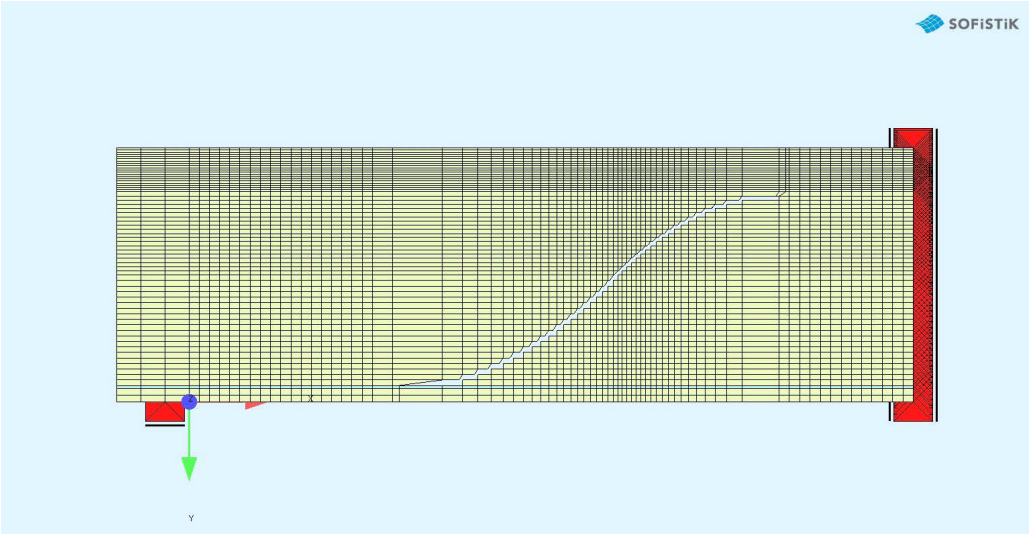

Figure 6. FEM Model without friction elements bridging the crack.

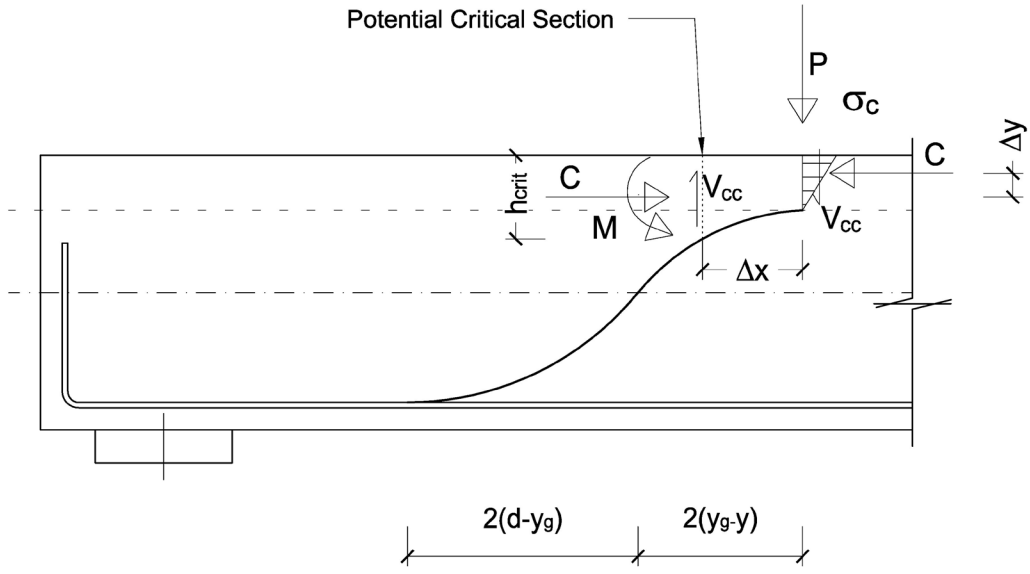

Figure 7. Failure section.

The constitutive laws of the horizontal and vertical springs are obtained using a kinematic assumption relating the crack width with the relative slip between crack lips. The assumption is that the points of the crack located above the centroid of the cross section rotate with respect to the top point of the crack (point B of Figure 4) while the points located below the centroid of the uncracked section rotate with respect to the bottom point of the crack (point A of Figure 4). This kinematic assumption is summarized in Figure 8. If θ is the rotation, the displacement of a point of the crack placed at a distance ρ from the point of rotation would be $\delta=\rho\theta$. From this value, the angle the crack forms with the horizontal (α) and the angle of the line that joins the point of the crack under consideration and the point of rotation with the vertical, β, it is possible to obtain the values of the crack opening (w) and the slip between the crack lips (Δ) (see Eq. (4)).

$$w = \delta\cos\left(\alpha + \beta - 90^{\circ}\right)$$
$$\Delta = \delta\sin\left(\alpha + \beta - 90^{\circ}\right) \tag{4}$$

Providing different values for θ, the values of w and Δ are obtained. With these values, the tangential (τ_w) and normal stresses (σ_w) can be determined by using Eq. (3) . The constitutive law of the horizontal and vertical truss elements can then be determined by projecting the stresses in these directions. Eq. (5) shows the corresponding expressions of the stress and strain defining the constitutive laws of the horizontal and vertical springs:

$$\sigma_x = \tau_w \cos\alpha + \sigma_w \sin\alpha$$
$$\varepsilon_x = \frac{(w \sin\alpha - \Delta \cos\alpha)}{dx}$$
$$\sigma_z = \tau_w \sin\alpha - \sigma_w \cos\alpha \tag{5}$$
$$\varepsilon_z = \frac{(w \cos\alpha - \Delta \sin\alpha)}{dz}$$

where:

- σ_x is the stress in the horizontal springs for a given value of the rotation
- ε_x is the strain in the horizontal springs for a given value of the rotation
- σ_z is the stress in the vertical springs for a given value of the rotation
- ε_z is the strain in the vertical springs for a given value of the rotation
- d_x is the initial horizontal distance between crack lips (initial length of horizontal truss elements)
- d_z is the vertical distance between finite elements at the location of the crack (initial length of the vertical truss elements)

The area of the truss elements is equal to the width of the section times the height of the corresponding finite element.

With this definition, tensile strength is accounted, since for strains smaller than the cracking stress, linear behaviour is assumed up to the cracking stress (see example given in Figure 9). Therefore even though the crack geometry is prefixed the element does not behave as if the crack were fully formed from the very beginning.

Figure 10 shows how the lips of the crack move with respect to each other according to the kinematic assumption made above. The displacement closely mirrors that observed in the FEM model and seems like a reasonable approximation to actual behaviour. This kinematic assumption should probably be modified for elements with longitudinal skin reinforcement since the crack width opening would be controlled locally at the level of the reinforcing bars. However, most real applications of elements without shear reinforcements (slabs, walls) do not have such reinforcement. In the figure the opening of the crack is plotted for two different effective heights and for the same rotation. Note how the crack opening is larger for the larger height. This will reduce the contribution of aggregate interlock for the same rotation and will automatically provide a size effect.

5. RESULTS

By using the model described in the previous section, the shear that is transferred by the uncracked compression chord, by aggregate interlock and by the dowel effect have been evaluated for test 70-3.1-2P-I. For this the "SIR cuts" feature of SOFISTIK has been used. This feature allows to make cuts in the structure and obtain normal and shear forces within the selected zone only. Thus, for example, it is possible to make a vertical cut at the section of the applied load over the full height of the section or limited to the height of the compression chord. The software integrates the forces within the cut and provides the normal force and the shear force corresponding to the stresses within the cut. In Figure 11, the normal and shear forces per meter are shown for the model which neglects the effect of aggregate interlock and compared with those of the model that considers aggregate interlock for 80% of the failure load. The comparison is made for 80% of the failure load because without aggregate interlock convergence was not achieved in the model without springs for the actual failure load. The behaviour of the model without aggregate interlock is that of a cracked section in flexure and most of the shear force is taken by the compressed chord. The shear stress distribution is quite similar to that of a linear elastic section with a height equal to the compressed height. For the model with aggregate interlock, however the behaviour is less clear, as significant shear stresses are also observed along the cracked part of the section, below the compressive chord. Note that the stress in the reinforcement is underestimated because, as explained above, the area of the steel was designed to provide the same out-of-plane stiffness as the actual reinforcement. This results in an overestimation of the steel area.

By using the "SIR cuts" feature, the shear taken by the compressed chord is determined by making a cut immediately to the left of the point of load application with a height equal to the height of the compressed chord. Then the shear force taken by dowel effect is determined by making a cut along the reinforcement at the bottom of the section, where the crack begins. Finally the contribution of aggregate interlock is determined by summing the forces in the nonlinear vertical truss elements. The results of this analysis are given in Table 1 and Figure 12. It can be seen that the sum of the three contributions does not always fully account for the applied load. This is due to imperfect convergence, but precision is nonetheless good enough. For low values

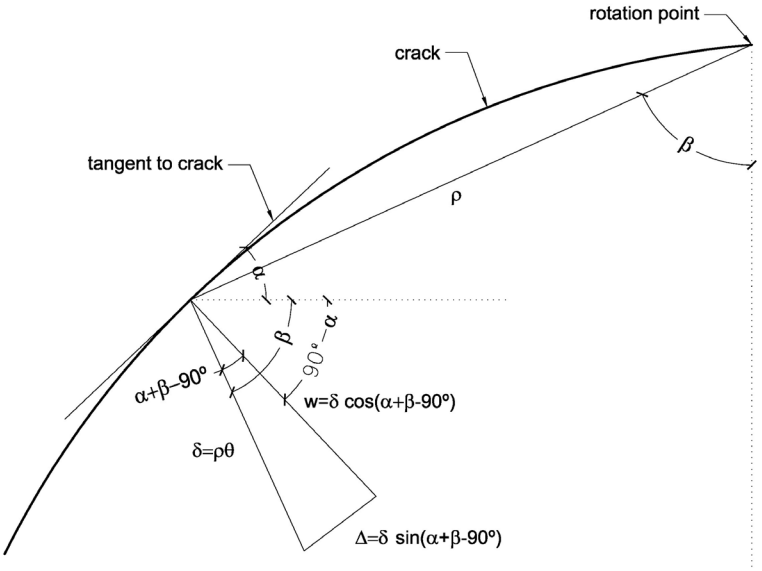

Figure 8. Kinematic assumption

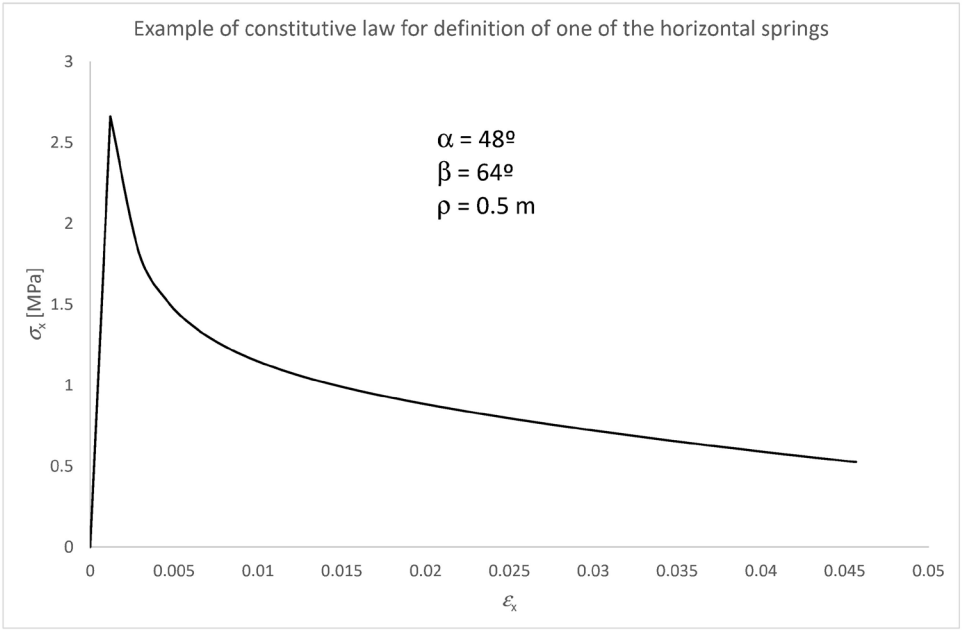

Figure 9. Example of constitutive law for one of the horizontal springs.

TABLE 1.
Distribution of shear between shear-resisting mechanisms for different load levels

% of ultimate load	V	V_{cc}	V_{agg}	V_{dowel}	$V_{cc}+V_{agg}+V_{dowel}$	% V	V_{cc}/V	V_{agg}/V	V_{dowel}/V
100%	**230**	**153.8**	**74.2**	**2.6**	230.6	100%	67%	32%	1%
80%	**184**	**117.7**	**56.5**	**5.1**	179.3	97%	66%	32%	3%
50%	**115**	**44.9**	**61.3**	**3.3**	109.5	95%	41%	56%	3%
25%	**57.5**	**18.5**	**37.0**	**0.9**	56.4	98%	33%	66%	2%

of shear, aggregate interlock is dominant, with still a significant contribution from the compressed chord. As the shear force increases, however, the contribution of aggregate interlock increases at a slower pace. This is logical as the increase in the crack width is unfavourable, even though the increase in slip mobilizes higher stresses. As a consequence of this complex non-linear behaviour the contribution of aggregate interlock stagnates, and the increase of the shear force is mostly taken by the compression chord. In all stages the contribution of dowel effect is very small. As explained above, failure comes about when the principal stress reaches the assumed tensile stress to the left of the applied load. The loss of the capacity of the compressed chord, which is taking 67% of the shear force at this stage cannot be compensated by an increase in aggregate interlock whose contribution has stagnated nor by

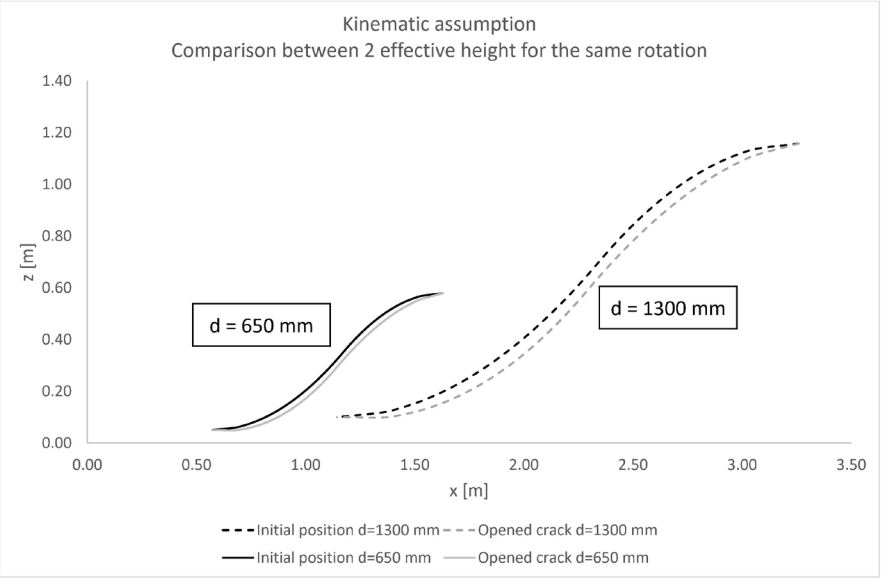

Figure 10. Movement of crack lips according the kinematic assumption made

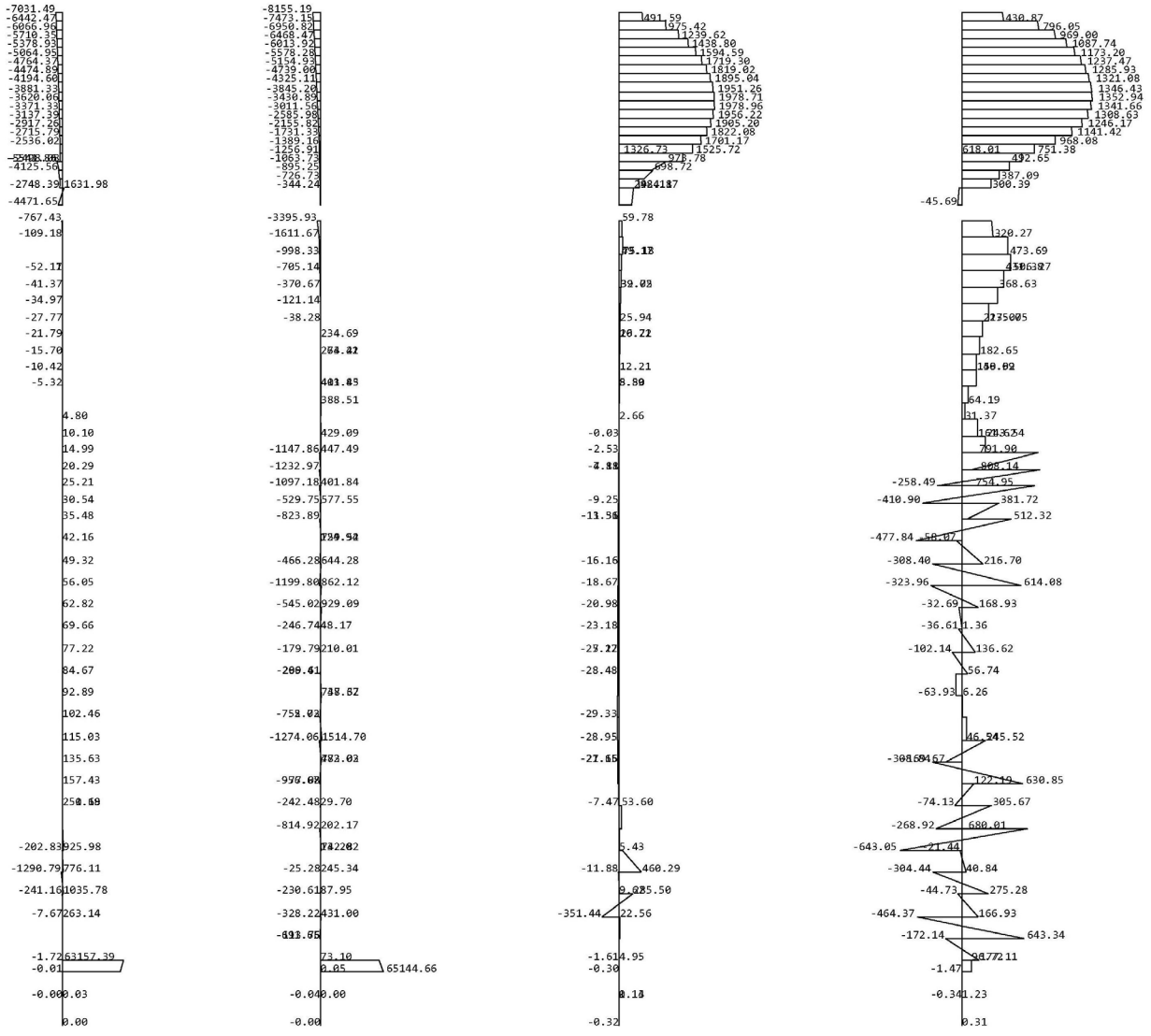

a) b) c) d)

Figure 11. Normal and shear forces, per meter, for 80% of the ultimate load applied in the model : a) normal stresses for model without aggregate interlock, b) normal stresses for model with aggregate interlock , c) shear stresses for model without aggregate interlock, and d) shear stresses for model with aggregate interlock

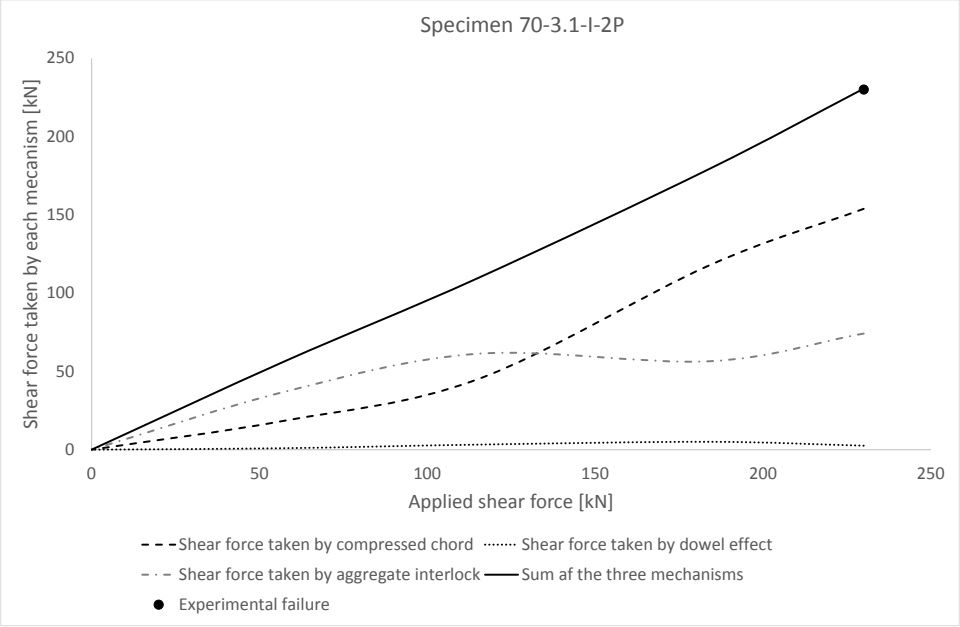

Figure 12. Distribution of shear between resistance mechanisms (shear taken by compressed chord, aggregate interlock, and dowel effect).

the dowel effect and a crack develops along the upper face of the tension reinforcement as failure occurs.

Of course the distribution of forces shown in Table 1 and Figure 12 should not be assumed to be general as it will vary depending on the specimen's geometry, reinforcement ratio, size, etc. See for example reference [23]. A future work to be carried out would be a systematic application of the model to specimens covering a wide range of different parameters.

Figure 10. Normal and shear forces, per meter, for 80% of the ultimate load applied in the model : a) normal stresses for model without aggregate interlock, b) normal stresses for model with aggregate interlock , c) shear stresses for model without aggregate interlock, and d) shear stresses for model with aggregate interlock

6. CONCLUSIONS

From the above considerations, the following preliminary conclusions, based on the analysis of a single test, can be drawn:

- A model to evaluate the shear resistance has been developed which can be implemented using FEM modelling. The model has been generated by a python computer code, making it easy to apply for different test cases. The shape of the crack can be easily modified to adapt to different cases, in particular cases in which a direct tension failure occurs and a straight crack is expected. Although the model has been applied to a single case, the prediction of the ultimate load is close to the measured ultimate load. For this, however, the effect of sustained loading on tensile strength had to be considered by reducing the tensile strength by 30% (k_{ct}=0.7) as suggested in FprEN 1992-1-1:2022 [24].
- The behaviour is complex, especially in what regards the contribution of aggregate interlock. The contribution of aggregate interlock is dominant for low values of the shear force but stagnates for higher values of the shear force because the increase in its value due to slip between crack lips is countered by the opening of the crack width. This, of course would imply that an element with longitudinal skin reinforcement would have a greater contribution of the aggregate interlock effect, although this is not a practical case for elements without stirrups.
- The contribution of the dowel effect is quite small throughout the loading process.
- For the case studied, the contribution of the compressed chord reached two-thirds of the shear force before failure. Failure comes about by tension failure (principal stress reaching the assumed sustained tensile strength) occurring to the left of the applied force in an area where a compressed cantilever subjected to a negative bending moment forms. This is compatible with vertical cracks appearing on the top chord to the left of the applied load.
- The model must be compared to other tests and should be tested for elements with a large contribution from direct strutting to see if it accounts for this effect adequately. Such analyses could form the basis for the formulation of a simplified model, which could be applicable for design purposes.

References

[1] A. Muttoni y M. Fernández Ruiz, «Shear Strength of Members without Transverse Reinforcement as Function of Critical Shear Crack Width,» *ACI Structural Journal*, vol. 105, nº 2, pp. 163-172, 2008.

[2] M. Collins, D. A. P. Mitchell y F. Vecchio, «A general shear design method,» *ACI Structural Journal*, vol. 93, nº 1, pp. 36-45, 1996.

[3] A. Marí, Cladera, A., J. Bairán, E. Oller y C. Ribas, «Shear-flexural strength mechanical model for the design and assessment of reinforced concrete beams subjected to point or distributed loads,» *Frontiers of Structural and Civil Engineering*, vol. 8, nº 4, pp. 337-353, 2014.

[4] R. Fenwick y T. Paulay, «Mechanism of Shear Resistance of Concrete Beams,» *ASCE Structural Journal*, vol. 94, pp. 2325-2350, 1968.

[5] H. Taylor, «The Fundamental Behavior Of Reinforced Concrete Beams In

Bending And Shear,» de SP-42 *Shear in Reinforced Concrete*, Detroit, ACI, 1974, pp. 43-77.

[6] H. Taylor, «Investigation of the Forces carried Across Cracks in Reinforced Concrete Beams in Shear by Interlock of Aggregate,» Cement and Concrete Association, London, 1970.

[7] J. Walraven, «Aggregate interlock: a theoretical and experimental investigation,» Delft University of Technology, Delft, 1980.

[8] J. Walraven, «Fundamental analysis of aggregate interlock,» *ASCE J. Struct. Div.*, vol. 107, nº 11, pp. 2245-2270, 1981.

[9] F. Cavagnis, M. Fernández Ruiz y A. Muttoni, «A mechanical model for failures in shear of members without transverse reinforcement based on the development of a critical shear crack,» *Eng. Struct.*, vol. 157, pp. 300-315, 2018.

[10] F. Vecchio y M. Collins, «Response of Reinforced Concrete to In-plane in Plane Shear and Normal Stresses. Publication No. 82-03,» University of Toronto, Toronto, 1982.

[11] W. Krefeld y C. Thruston, «Contribution of Longitudinal Steel to Shear Resistance of Reinforced Concrete Beams,» *ACI Structural Journal*, vol. 63, nº 3, pp. 325-344, 1966.

[12] T. Baumann y H. Rüsch, «Versuche zum Studium der Verdübelungswirkung derBiegezugbewehrung em es Stahbetonbalkens, DAfStb H210,» Wilhelm und Sohn, Berlin, 1970.

[13] G. Kani, «The Riddle of Shear Failure and its Solution,» *ACI Structural Journal*, vol. 61, nº 4, pp. 441-467, 1964.

[14] K. Reineck, «Ultimate shear force of structural concrete members without transverse reinforcement derived form a mechanical model,» *ACI Structural Journal*, vol. 88, nº 5, pp. 592-602, 1991.

[15] A. Monserrat López, «Comportamiento frente a cortante de vigas continuas de hormigón armado: estudio experimental de los mecanismos resistentes y de la influencia de la cinemática desarrollada en combinación con los esfuerzos de flexión. PhD Thesis.,» Universitat Politècnica de València, Valencia, 2020.

[16] L. Montoya-Coronado, C. Ribas, J. Ruiz-Pinilla y A. Cladera, «Time-history analysis of aggregate interlock in reinforced concrete beams without stirrups,» *Engineering Structures*, vol. 283, p. 115912, 2023.

[17] A. Frontera y A. Cladera, «Long-term shear strength of RC beams based on a mechanical model that considers reinforcing steel corrosion,» *Structural Concrete*, vol. 24, pp. 25-40, 2023.

[18] M. Pejatović, M. Ruiz y A. Muttoni, «Design of slender and squat reinforced concrete members with shear reinforcement2023,» *Structural Concrete*, vol. 24, nº 1, p. 985– 1001, 2023.

[19] Miguel, P., Fernández, M., Hegger, J., & Schmidt, M. (2023). Shear Resistance of Members Without Shear Reinforcement in Presence of Compressive Axial Forces in the Next Eurocode 2. *Hormigón y Acero*, 74(299-300), 41-60. https://doi.org/10.33586/hya.2023.3112

[20] G. Quaranta, D. De Domenico y M. G., «Machine-learning-aided improvement of mechanics-based code-conforming shear capacity equation for RC elements with stirrups,» *Engineering Structures*, vol. 267, p. 114665, 2022.

[21] T. Jayasinghe, T. Gunawardena y P. Mendis, «Assessment of shear strength of reinforced concrete beams without shear reinforcement: A comparative study between codes of practice and artificial neural network,» *Case Studies in Construction Materials*, vol. 16, p. e01102, 2022.

[22] P. Padilla Lavaselli, «Influencia de la distribución de la carga en la capacidad resistente a cortante en elementos sin armadura transversal : estudio teórico y experimental (Tesis Doctoral),» UPM, Madrid, 2009.

[23] F. Cavagnis, M. Fernández Ruiz y A. Muttoni, « An analysis of the shear-transfer actions in reinforced concrete members without transverse reinforcement based on refined experimental measurements,» *Structural Concrete. 2018; 19: 49– 64*. https://doi.org/10.100, vol. 19, pp. 49-64, 2018.

[24] Comité Européen du Béton (CEN), FprEN 1992-1-1:2022 Eurocode 2: Design of concrete structures — Part 1-1: General rules Rules for buildings, bridges and civil engineering structures, Brussels: CEN, 2022.